Accepted Manuscript

Title: Electrospun composite cellulose acetate/iron oxide nanoparticles non-woven membranes for magnetic hyperthermia applications

Authors: Ricardo J.R. Matos, Catarina I.P. Chaparro, Jorge C. Silva, Manuel Almeida Valente, João Paulo Borges, Paula I.P. Soares

Please cite this article as: Matos RJR, Chaparro CIP, Silva JC, Valente MA, Borges JP, Soares PIP, Electrospun composite cellulose acetate/iron oxide nanoparticles non-woven membranes for magnetic hyperthermia applications, *Carbohydrate Polymers* (2018), https://doi.org/10.1016/j.carbpol.2018.06.048

Electrospun composite cellulose acetate/iron oxide nanoparticles non-woven membranes for magnetic hyperthermia applications

Ricardo J. R. Matos[1], Catarina I. P. Chaparro[1], Jorge C. Silva[2], Manuel Almeida Valente[3], João Paulo Borges[1*], Paula I. P. Soares[1*]

[1]CENIMAT/i3N, Departamento de Ciência dos Materiais, Faculdade de Ciências e Tecnologia, FCT, Universidade Nova de Lisboa, 2829-516 Caparica, Portugal

[2]CENIMAT/i3N, Departamento de Física, Faculdade de Ciências e Tecnologia, FCT, Universidade Nova de Lisboa, 2829-516 Caparica, Portugal

[3]Physics Department (I3N), University of Aveiro, Campus Universitário de Santiago, Aveiro, Portugal.

[1*]**Address correspondance to this author at** CENIMAT/i3N, Departamento de Ciência dos Materiais, Faculdade de Ciências e Tecnologia, FCT, Universidade Nova de Lisboa, 2829-516 Caparica, Portugal; Tel: +351 21 2948564; Fax: +351 21 2947810; e-mail: pi.soares@fct.unl.pt, jpb@fct.unl.pt.

HIGHLIGHTS

- Composite membranes for magnetic hyperthermia were produced;
- Magnetite nanoparticles were combined with cellulose acetate membranes;
- Adsorption method originates composite membranes with higher heating ability;
- Incorporation method improves mechanical properties of composite membranes;

ABSTRACT

In the present work composite membranes were produced by combining magnetic nanoparticles (NPs) with cellulose acetate (CA) membranes for magnetic hyperthermia

applications. The non-woven CA membranes were produced by electrospinning technique, and magnetic NPs were incorporated by adsorption at fibers surface or by addition to the electrospinning solution. Therefore, different designs of composite membranes were obtained. Superparamagnetic NPs synthesized by chemical precipitation were stabilized either with oleic acid (OA) or dimercaptosuccinic acid (DMSA) to obtain stable suspensions at physiological pH. The incorporation of magnetic NP into CA matrix was confirmed by scanning and transmission electron microscopy. The results showed that adsorption of magnetic NPs at fibers' surface originates composite membranes with higher heating ability than those produced by incorporation of magnetic NPs inside the fibers. However, adsorption of magnetic NPs at fibers' surface can cause cytotoxicity depending on the NPs concentration. Tensile tests demonstrated a reinforcement effect caused by the incorporation of magnetic NPs in the non-woven membrane.

KEYWORDS

Cellulose acetate; composite membranes; electrospinning; fibers; iron oxide nanoparticles; magnetic hyperthermia.

INTRODUCTION

Cancer is a major public health problem worldwide causing nearly 1 in 6 deaths, from which 70% occur in low- or middle-income countries. Chemotherapy has a limited effectiveness, poor distribution and lack of selectivity. Alternatively, magnetic hyperthermia is clinically used as a treatment for various human solid cancers (Assa et al., 2017; Shi et al., 2017; Yan et al., 2018). Cancer cells are more sensitive to temperature oscillations than normal cells due to reduced blood flow in the tumor site. Therefore, temperatures around 42-43ºC can cause significant tumor cell death without harming healthy tissues (Kobayashi, 2011; Majewski et al., 2007). The use of magnetic NPs could be an innovative solution to perform magnetic hyperthermia. Magnetic NPs can function at cellular and molecular level of biological interactions and can be manipulated using a magnetic field (Yadollahpour et al., 2016; Zhong et al., 2015). The application of free magnetic NPs has several limitations due to low solubility, poor cancer targeting, and

2

leakage of NPs from the tumor location. For that reason, a strategy currently being researched involves NPs-loaded electrospun nanofibers for localized magnetic hyperthermia, which is the main purpose of this work (Lee et al., 2015). Magnetite nanoparticles (Fe_3O_4) have attracted broad interest for cancer treatment using magnetic hyperthermia because they are non-toxic and biocompatible (Darwish et al., 2016). In general, iron oxide nanoparticles (IONPs) become superparamagnetic at room temperature when their size is below about 15 nm, and heat generation is a result of a combination of internal Néel fluctuations of the particle magnetic moment and the external Brownian fluctuations (Wu et al., 2015). However, aggregation among superparamagnetic IONPs is a common phenomenon (Mahdavi et al., 2013). Hence, for protecting bare IONPs against aggregation, coating agents such as OA and DMSA can be used, without significantly affect their magnetic properties (Soares et al., 2015b; Soares et al., 2014b).

Electrospinning is a simple, fast and easy to scale-up technique to produce functional materials based on polymeric micro/nanofibers with high surface-to-volume ratio and tunable porosity (Baptista et al., 2013; Baptista et al., 2011). Electrospinning can be used to produce stimuli-responsive fibers that actively react to changes in the surrounding environment, which are translated into significant changes in their morphological and chemical properties (Almeida et al., 2012). Combining electrospun non-woven membranes with magnetic NPs produces a flexible composite system with fixed NPs suitable for magnetic hyperthermia applications. In addition, this combination can improve cell adhesion, proliferation, and differentiation when a magnetic field is applied (Rao et al., 2017). The composite membranes produced in this work are composed by an electrospun matrix of cellulose acetate and functionalized with magnetite NPs. The NPs were conjugated to the polymeric matrix either through adsorption, or by incorporation in the electrospinning solution. Some authors have explored the use of electrospinning to produce controlled drug delivery systems (Aguilar et al., 2017; Qiu et al., 2013; Thakkar et al., 2017), while a few studies encapsulated IONPs into polymeric nanofibers for magnetic hyperthermia application (Lin et al., 2012; Lin et al., 2013; Zhong et al., 2015). This combination will cause a synergistic effect, thus producing a highly efficient cancer treatment option for easy to access tumors or post-operation treatments, with smaller drug dose and a significant reduction of side effects.

3

EXPERIMENTAL SECTION

All the chemical reagents used in this research work were of analytical grade and used without further purification.

Synthesis of iron oxide nanoparticles

Iron oxide nanoparticles were produced by a chemical co-precipitation technique using a previously described method (Soares et al., 2014a; Soares et al., 2015a; Soares et al., 2016a). IONPs without further treatment will be named "Bare-Fe_3O_4 NPs"; the ones stabilized with either DMSA (*Sigma- Aldrich*) 4% or OA (*Fisher Chemical*) 64 mM will be named "DMSA-Fe_3O_4 NPs" and "OA-Fe_3O_4 NPs", respectively.

IONPs stabilization with OA was performed by adding to the NPs suspension an appropriate amount of OA calculated as a percentage of the NPs mass. The mixture reacted for 1 h in an ultrasound bath. In the case of coating with DMSA, the suspension pH was previously adjusted to pH 3 with nitric acid 65% under magnetic stirring. DMSA was added immediately at a 3–4 ratio of [DMSA]/[Fe^{2+}]. DMSA was dissolved in 2 mL of deionized water and the pH adjusted to 5.5 with 0.1 M NaOH solution under vigorous stirring (Fauconnier et al., 1997; Massart, 1980). The reaction of DMSA with IONPs was performed in an ultrasound bath during 1 h. In both cases, a part of the suspension was freeze-dried (VaCo2, *Zirbus*) to obtain dry NPs for further characterization.

Production of CA/Fe_3O_4 composite

To produce CA/Fe_3O_4 composites, two strategies were used: i) Immersion of CA membrane into IONPs solution using different concentrations – Adsorption; ii) electrospinning a solution containing CA and IONPs – Incorporation.

Adsorption of IONPs in CA membranes

A 12 wt% CA solution in 2:1 (w/w) acetone (*Fisher chemical*)/N, N- dimethylacetamide (DMAc, *Sigma-Aldrich)* was prepared and used for electrospinning. Electrospinning was performed at 20ºC with humidity around 40%. The polymer solution was placed in a 1 mL syringe, and dispensed by a syringe pump (*KDS100*, *KD Scientific)* at a rate of 0.15 mL.h^{-1}. A high voltage supply (*Glassman EL 30kV*) was connected to the metallic needle (ITEC 21G) with a fixed voltage of 20 kV, and a sheet of aluminum foil was placed 17 cm in front of the tip of the needle to collect the fibers. The electrospun fiber mats were dried at room temperature for 24 h to remove any residual solvent. These parameters were based on the literature (Baptista et al., 2011; Tarus et al., 2016). However, other

4

combinations of parameters were tested. **Table 1** presents the electrospinning parameters tested that resulted in fibers without defects.

To produce CA/Fe_3O_4 composites by adsorption, the CA solution was electrospun during 6 h. CA membranes were cut into 2.5x1.5 cm pieces and placed in IONPs solution during 24 h in an orbital shaker. The adsorption method was tested using two concentrations of IONPs, 0.5 and 2.0 $mg.ml^{-1}$, either of DMSA-Fe_3O_4 NPs or OA-Fe_3O_4 NPs. The membranes were washed with ultrapure water to remove the non-adsorbed NPs and were dried at room temperature.

Incorporation of IONPs in CA nanofibers

In this case, a new solvent combination for CA was used: 63: 32: 5 (w/w/w) acetone/ DMAc/ IONPs solution ([OA-Fe_3O_4 NPs] = 6.34 $mg.ml^{-1}$; [DMSA-Fe_3O_4 NPs] = 4.01 $mg.ml^{-1}$). The addition of IONPs to CA solution affected its viscosity, and consequently the optimal conditions for electrospinning also change, as shown in **table 2.**

Characterization

The iron content of the samples was determined using the 1,10-phenantroline colorimetric method (Talelli et al., 2009). To obtain NPs concentration the formula $[Fe] = 0.7 \times [NPs]$ was used, obtained from control experiments.

Transmission electron microscopy (TEM) images were obtained using a Hitachi H-8100 II with thermo-ionic emission LaB_6 with a resolution of 2.7 Å. TEM analysis was performed in NPs diluted in pure water placed in a Kevlar 25 mesh grid. The membranes analysis was performed on the thinnest membrane that can be technically extracted.

The crystalline phases of the samples were verified using powder X-ray diffraction (XRD). X'Pert PRO PANAlytical X-ray diffractometer was used to obtain X-ray diffraction patterns of the iron oxide nanoparticles previously freeze-dried. The 2θ values were taken from 15º to 80º using a Cu-Kα radiation (λ = 1.54060 Å) with a step size of 0.033. The Scherrer's equation was used to measure the average crystallite size.

FTIR spectra of the samples were obtained using a Nicolet 6700–Thermo Electron Corporation Attenuated Total Reflectance- Fourier Transform Infrared spectrometer

(ATR-FTIR). Measurements were performed in freeze-dried samples in the range of 480–4000 cm^{-1} with a resolution of 2 cm^{-1}.

Dynamic Light Scattering (DLS) measurements were performed using a SZ-100 nanopartica series (Horiba, Lda) with a 532 nm laser and a Peltier temperature control system (25ºC). DLS measurements were carried out for diluted NPs suspensions (five samples for each concentration) using a disposable cell with a scattering angle equal to 90º. Data analysis was performed using cumulants statistics to measure hydrodynamic diameter (D_H) and polydispersity index (PDI) (Soares et al., 2016b).

Scanning electron microscopy (SEM) that allowed fiber morphology analysis was performed using a Carl Zeiss Auriga SEM equipment. The samples were coated with a thin layer of gold.

The magnetic properties of bare-Fe_3O_4 NPs and OA-Fe_3O_4 NPs were performed in previous studies (Soares et al., 2016b) using a 7 T SQUID magnetometer (S700X; Cryogenic Ltd.). The magnetization curves were obtained at 5 K and 320 K, with a variation of the applied field of -5 T up to 5 T. The magnetic properties of DMSA-Fe_3O_4 NPs was performed through Vibrating Sample Magnetometer (VSM) technique using a 10 T VSM magnetometer (Cryogenic-Cryofree). The magnetization curve was obtained at 300 K, with a variation of the applied field of -2 T up to 2 T.

Mechanical response – tensile tests

The tensile tests were performed on a Rheometric Scientific uniaxial tensile testing machine with 20 N load cell and operable through the Minimat software (Minimat Control Software Version 1.60 February 1994 (c) PL Thermal Science 1984-94 Reometric Scientific Ltd.). A velocity of 1 $mm.min^{-1}$ was applied in all experiments, which were performed at room temperature and humidity around 50%. For each type of membrane at least 10 samples were measured.

Cytotoxicity assays

To evaluate the cytotoxicity of the membranes, the assays were performed according to standard ISO-10993 Biological evaluation of medical devices, Part 5: Tests for in vitro cytotoxicity. The assays were performed using the extract method and Vero cells (monkey renal epithelial cells). To produce the extract, different samples were cut to have an identical mass of 5 mg and pre-sterilized with UV irradiation for 1 h. Each sample was placed in 1 mL of Dulbecco's modified Eagle's medium (DMEM, *Sigma Aldrich*) at 37ºC for 48 h.

6

Cells were seeded at a density of 20,000 cell.cm^{-2} in 96-well plates and grown in DMEM supplemented with 10% fetal bovine serum, 1% Penicilin-Streptomycin, sodium pyruvate (100 mM, *Life-Technologies*), and GlutaMAX^{TM} Supplement (*Life-Technologies*) followed by incubation at 37°C in 5% CO_2 during 24 h. Four concentrations of the extract were used: 5, 2.5, 1.25 and 0.625 mg.mL^{-1}. For each concentration, 5 replicas were performed. After this period, the medium was removed and a resazurin solution containing 90% of complete culture medium, as described above, and 10% of a 0.2 mg.mL^{-1} resazurin solution in PBS was added to each well. After 2 h incubation, the absorbance was measured at 570 and 600 nm. Negative control cells were incubated with complete medium. Positive control cells were treated with 10% DMSO to cause cell death. Cell viability is expressed as a percentage of the negative control, given by [% cell viability = treated cells/control cells x 100].

Magnetic hyperthermia assays

Magnetic hyperthermia measurements were obtained using a DM100 series from Nb Nanoscale Biomagnetics apparatus. The heating ability of 10 mg of each membrane loaded with IONPs was measured using an alternating current (AC) magnetic field of 24 kA.m^{-1}, with a frequency of 418.5 kHz for 10 min. Each sample was immersed in 1 mL of ultrapure water during the tests.

RESULTS AND DISCUSSION

Iron oxide nanoparticles

The colloidal stability of IONPs depends on two main factors: i) NPs size which must be small enough to prevent precipitation; ii) surface charge and chemistry that should prevent NPs aggregation through steric and coulombic repulsions (Yadollahpour et al., 2016). Consequently, the low stability of IONPs in aqueous medium requires the use of surfactants. To evaluate the morphology and size distributions of bare-NPs and coated NPs (DMSA-Fe$_3$O$_4$ NPs and OA-Fe$_3$O$_4$ NPs), TEM analysis was performed (**fig. 1**). Using the chemical precipitation technique, monodisperse bare-NPs with an average diameter of 9.4 ± 1.9 nm were obtained. When coated with either DMSA or OA, IONPs kept their spherical shape with average diameters of 9.8 ± 2.5 nm and 10.2 ± 2.4 nm were obtained for OA-Fe$_3$O$_4$ NPs and DMSA-Fe$_3$O$_4$ NPs, respectively, showing the surfactant did not significantly affect the average size of IONPs.

7

Fig. 1 G shows the XRD patterns of bare-Fe_3O_4 NPs, OA-Fe_3O_4 NPs and DMSA-Fe_3O_4 NPs. The characteristic peaks of magnetite were observed at 2θ of 30.1, 35.5, 43.2, 53.5, 57.0 and 62.8° corresponding to the diffraction planes (220), (311), (400), (422), (511) and (440), respectively. The positions and relative intensities of the reflection peaks of samples agree with the XRD diffraction peaks of standard Fe_3O_4 samples (JCPDS 00-019-0629 for magnetite and JCPDS 00-039-1346 for maghemite), indicating the synthesized NPs have a crystalline cubic magnetite structure. XRD data suggest the effect of surfactants on the crystal structure of Fe_3O_4 NPs is negligible. The average crystallite size (τ) of NPs was calculated from the full width at half-maximum (FWHM) of the most intense peak using the Scherrer's equation $\tau = K\lambda / (\beta cos\theta)$, where k is the grain shape factor ($K = 0.94$), λ is the incident X-ray wavelength, β is the FWHM (in radians) of the highest intensity, and θ is the corresponding diffraction angle. Bare-Fe_3O_4 NPs and coated NPs have similar average crystallite size of 9.75 nm. These results agree with the average diameter measured in TEM images.

To get further insight on IONP surface chemistry, bare and coated Fe_3O_4 NPs were characterized by FTIR spectroscopy (**Fig. 1 H).** Bare-Fe_3O_4 NPs show the three characteristic bands of Fe_3O_4: at 560 cm^{-1} the Fe-O stretching vibration mode, and at 1630 cm^{-1} and 3400 cm^{-1} the O-H stretching vibration modes (Yang et al., 2010). In the OA-Fe_3O_4 NPs FTIR spectrum six new bands at 1407, 1434, 1521, 1710, 2849 and 2921 cm^{-1} appeared. The bands at 2849 and 2921 cm^{-1} are attributed to the asymmetric CH_2 stretch and the symmetric CH_2 stretch in OA, respectively. The band at 1407 cm^{-1} corresponds to CH_3 umbrella mode of OA. The band at 1710 cm^{-1}, corresponding to stretching vibration of C=O, is also characteristic of OA. The spectrum also indicates the presence of two bands, 1434 cm^{-1} (ν_s: COO$^-$) and 1521 cm^{-1} (ν_{AS}: COO$^-$), attributed to the oleate ion immobilized on the magnetite surface (Mahdavi et al., 2013). In the DMSA-Fe_3O_4 NPs spectrum, the new well-defined bands at 1570 and 1390 cm^{-1} appear, typical from asymmetric and symmetric stretching of carboxylate, respectively (Valois et al., 2010). The sharp carbonyl absorption bands present around 1700 cm^{-1} in DMSA was shifted to lower frequencies because the ligands are bound to the particles and their carboxyl group is dissociated and coordinated with the iron oxide surface (Palma et al., 2015). The band at 1011 cm^{-1} is attributed to the C-O ether stretch (Valois et al., 2010). Given the large splitting between the –COO$^-$ bands, the carboxylate group appears to be bound to iron through a monodentate interaction (Chen et al., 2008; Ge et al., 2009; Palma et al., 2015).

DLS measurements were performed in OA-Fe_3O_4 NPs and DMSA-Fe_3O_4 NPs to evaluate their stability in physiological conditions. **Fig. 2 A** and **B** represents the two groups of calculated D_H for OA-Fe_3O_4 NPs and DMSA-Fe_3O_4 NPs, respectively. The average sizes determined at pH 7 (physiological pH) were 140 ± 13 nm and 79 ± 11 nm for OA-Fe_3O_4 NPs, and 164 ± 13 nm and 101 ± 9 nm for DMSA-Fe_3O_4 NPs. The PDI was around 0.2 for every experimental curve obtained, indicating a fairly monodisperse suspension.

Magnetic measurements were performed to evaluate the influence of OA and DMSA in Fe_3O_4 NPs magnetic properties. Magnetic saturation values are presented in emu per gram of the whole particle (including magnetic and non-magnetic material). **Fig. 2 C** shows the hysteresis loops of bare-Fe_3O_4 NPs, OA-Fe_3O_4 NPs and DMSA-Fe_3O_4 NPs above the blocking temperature. In this temperature range the samples are superparamagnetic (absence of coercivity and remanence) with differences in their saturation magnetization (M_S): 58 emu.g^{-1} for both bare and DMSA-Fe_3O_4 NPs, and 46 emu.g^{-1} for OA-Fe_3O_4 NPs. The reduction of Fe_3O_4 M_S is dependent upon oleic acid percentage (Soares et al., 2014a; Soares et al., 2016b).

CA-Magnetite composites

To obtain magnetic membranes suitable for magnetic hyperthermia applications, an efficient incorporation of IONPs into CA membranes is crucial. SEM images of the electrospun fiber mats before and after 24 h of adsorption in solutions with concentration of 2.0 mg.ml^{-1} of OA-Fe_3O_4 NPs or DMSA-Fe_3O_4 NPs are shown in **Fig. 3**. The electrospun CA nanofibers have smooth morphology, bead-free and an average diameter of about 300 nm, which was kept even after 24 h in adsorption medium. The high surface area of electrospun fibers enhances the binding of IONPs. With the increase of Fe_3O_4 NPs concentration, an increase in the NPs amount at the CA fibers surface is visible. DMSA-Fe_3O_4 NPs demonstrated more affinity to binding to CA fibers surface than OA-Fe_3O_4 NPs, for the same NPs concentration

The other method to produce composite membranes was through incorporation of Fe_3O_4 NPs in the electrospinning solution. Since the incorporation of Fe_3O_4 NPs in CA solution changed its viscosity, the electrospinning parameters were changed. **Fig. 4** shows SEM images of both CA/OA-Fe_3O_4 (A) and CA/DMSA-Fe_3O_4 (B) composite membranes produced by this method. The presence of Fe_3O_4 NPs in the electrospinning solution does not change the morphology of CA fibers, which kept their cylindrical shape. However, compared to plain CA, the fiber diameter was reduced from 272 ± 72 nm (CA fibers

produced with 63: 32: 5 (w/w/w) acetone/ DMAc/ water solution) to 165 ± 55 nm and 161 ± 34 nm with the incorporation of OA- and DMSA-Fe_3O_4 NPs, respectively. The fiber diameter decrease may be related not only to the effect of Fe_3O_4 NPs in the solution viscosity, but also due to the change in the electrospinning parameters.

When composite CA/Fe_3O_4 membranes are produced by adsorption of Fe_3O_4 NPs, the NPs are clearly visible at the fiber surface. However, when using the incorporation technique, Fe_3O_4 NPs are not visible at the fiber surface. To confirm the presence of Fe_3O_4 NPs in composite membranes, TEM images were obtained. **Fig. 5** shows Fe_3O_4 NPs organized as clusters (probably caused by the agglomeration of NPs) inside CA fibers.

Mechanical response – tensile tests

The different types of CA membranes functionalized with Fe_3O_4 NPs were submitted to stress-strain assays (**Fig. 6**). All samples exhibited a similar mechanical behavior under tensile forces whereas a major region of elastic deformation and a very reduced region of plastic deformation is visible. This behavior is characteristic of fragile materials. With the incorporation of Fe_3O_4 NPs, plastic deformation of the composite membranes is almost negligible since membrane rupture occurs almost immediately. Three parameters that characterize the membranes were obtained from the curves of the tensile tests: Young's Modulus (E), which characterizes the mechanical strength of the material; the elastic limit stress (σ_{EL}); and the ultimate tensile strength (UTS). The results for each membrane are shown in **Fig. 6** C. In all composite membrane types, an improvement of the membrane's mechanical parameters with the incorporation of Fe_3O_4 NPs, compared to the plain CA membrane, is visible. The Young's modulus increases by a factor between 3 and 4 for all membrane containing IONPs, assuming values in the 30 to 40 MPa interval. The type of Fe_3O_4 NPs coating does not seem to affect the mechanical response of the membranes, since E increases in the same proportion for all membranes types. In conclusion, the incorporation of IONPs has a reinforcing effect on the membranes.

Cytotoxicity assays

Cytotoxicity assays were performed to evaluate the cytotoxic effect of IONPs incorporated on CA membranes. **Fig. 7** shows cell viability after incubation with 10 mg of each type of membrane studied. The results show that only CA/DMSA-Fe_3O_4 membrane coated in a solution containing a NPs concentration of 2.0 mg.mL^{-1} exhibits cytotoxicity due the large quantity of DMSA-Fe_3O_4 NPs adsorbed on CA fibers (Ge et al., 2013; Ge et al., 2009). The other composite membranes showed almost 100%

10

viability. The results allow to conclude that NPs may be cytotoxic when present at higher concentrations. Therefore, the concentration, type of incorporation in fibers and rate of IONPs released to the medium should be carefully studied and adjusted to avoid cytotoxic effects and to guarantee the biocompatibility of the membranes. However, for the conditions used in this work, cell viability did not reach critical values.

Magnetic hyperthermia assays

Magnetic hyperthermia assays were performed to evaluate the heating ability of IONPs incorporated in CA membranes. **Fig. 8** represents the temperature variation during the assays for each type of membrane studied. The highest temperature variation occurred for the membranes with DMSA-Fe_3O_4 NPs adsorbed at fibers surface method. Adsorption of Fe_3O_4 NPs using concentrations of 0.5 mg.ml^{-1} and 2.0 mg.ml^{-1}, resulted in an average temperature variation of 5.1°C and 11.5°C, respectively. These results agree with the higher adsorption capacity of the DMSA-Fe_3O_4 NPs to CA fibers, compared to OA-Fe_3O_4 NPs. In OA-Fe_3O_4 NPs using concentrations of 0.5 mg.ml^{-1} and 2.0 mg.ml^{-1}, resulted in an average temperature variation of 1.6°C and 2.4°C, respectively. Magnetic hyperthermia measurements of composite membranes produced by incorporation of Fe_3O_4 NPs resulted in very small temperature variation, smaller than 1°C. In this case, the amount of Fe_3O_4 NPs incorporated should be increased to produce clinically relevant temperature variations. Being the normal body temperature 37°C, a temperature variation of five degrees is enough to achieve a therapeutic value for the cancerous tissue (about 42°C). This therapeutic temperature can be reached by adjusting the NPs coating, concentration within the membrane, and the method of NPs incorporation, as shown in the results.

CONCLUSIONS

We report here the fabrication and characterization of electrospun cellulose acetate mats functionalized with superparamagnetic magnetite nanoparticles. These composites exhibited good heating properties under an alternating magnetic field, which make them suitable for magnetic hyperthermia applications. The nanoparticles revealed a superparamagnetic behavior as intended for biomedical applications. By varying the concentration of Fe_3O_4 NPs present on cellulose acetate mats, and by modelling the

conditions of the hyperthermia assay, it is possible to reach therapeutic temperatures. Tensile tests indicate that the addition of Fe_3O_4 NPs has a significant impact on the cellulose acetate mechanical response, increasing Young's Modulus, the elastic limit stress and the ultimate tensile strength. Regarding *in vitro* experiments, the concentration of Fe_3O_4 NPs in composite membranes should be modulated to achieve clinically relevant heat without causing cytotoxic effects, which could harm the surrounding healthy tissues. Composite membranes with incorporated DMSA-Fe_3O_4 NPs through adsorption in a solution with concentration of 0.5 mg.ml^{-1}, revealed the most promising for use in magnetic hyperthermia, considering the heating ability and the absence of cytotoxicity.

ACKNOWLEDGMENTS

REFERENCES

Aguilar, L. E., GhavamiNejad, A., Park, C. H., & Kim, C. S. (2017). On-demand drug release and hyperthermia therapy applications of thermoresponsive poly-(NIPAAm-co-HMAAm)/polyurethane core-shell nanofiber mat on non-vascular nitinol stents. *Nanomedicine, 13*(2), 527-538.

Almeida, H., Amaral, M. H., & Lobão, P. (2012). Temperature and pH stimuli-responsive polymers and their applications in controlled and self-regulated drug delivery. *Journal of Applied Pharmaceutical Science, 2*(6), 1-10.

Assa, F., Jafarizadeh-Malmiri, H., Ajamein, H., Vaghari, H., Anarjan, N., Ahmadi, O., & Berenjian, A. (2017). Chitosan magnetic nanoparticles for drug delivery systems. *Crit Rev Biotechnol, 37*(4), 492-509.

Baptista, A., Soares, P., Ferreira, I., & Borges, J. P. (2013). Nanofibers and Nanoparticles in Biomedical Applications. In A. Tiwari & A. Tiwari (Eds.). *Bioengineered Nanomaterials* (pp. 98-100). New York: CRC Press.

Baptista, A. C., Martins, J. I., Fortunato, E., Martins, R., Borges, J. P., & Ferreira, I. (2011). Thin and flexible bio-batteries made of electrospun cellulose-based membranes. *Biosensors and Bioelectronics, 26*(5), 2742-2745.

Chen, Z. P., Zhang, Y., Zhang, S., Xia, J. G., Liu, J. W., Xu, K., & Gu, N. (2008). Preparation and characterization of water-soluble monodisperse magnetic iron oxide nanoparticles via surface double-exchange with DMSA. *Colloids and Surfaces a-Physicochemical and Engineering Aspects, 316*(1-3), 210-216.

Darwish, M. S., Nguyen, N. H., Sevcu, A., Stibor, I., & Smoukov, S. K. (2016). Dual-modality self-heating and antibacterial polymer-coated nanoparticles for magnetic hyperthermia. *Mater Sci Eng C Mater Biol Appl, 63*, 88-95.

Fauconnier, N., Pons, J. N., Roger, J., & Bee, A. (1997). Thiolation of Maghemite Nanoparticles by Dimercaptosuccinic Acid. *J Colloid Interface Sci, 194*(2), 427-433.

Ge, G., Wu, H., Xiong, F., Zhang, Y., Guo, Z., Bian, Z., Xu, J., Gu, C., Gu, N., Chen, X., & Yang, D. (2013). The cytotoxicity evaluation of magnetic iron oxide nanoparticles on human aortic endothelial cells. *Nanoscale Res Lett, 8*(1), 215.

Ge, Y., Zhang, Y., Xia, J., Ma, M., He, S., Nie, F., & Gu, N. (2009). Effect of surface charge and agglomerate degree of magnetic iron oxide nanoparticles on KB cellular uptake in vitro. *Colloids Surf B Biointerfaces, 73*(2), 294-301.

Kobayashi, T. (2011). Cancer hyperthermia using magnetic nanoparticles. *Biotechnol J, 6*(11), 1342-1347.

Lee, H. J., Lee, S. J., Uthaman, S., Thomas, R. G., Hyun, H., Jeong, Y. Y., Cho, C. S., & Park, I. K. (2015). Biomedical Applications of Magnetically Functionalized Organic/Inorganic Hybrid Nanofibers. *Int J Mol Sci, 16*(6), 13661-13677.

Lin, T.-C., Lin, F.-H., & Lin, J.-C. (2012). In vitro feasibility study of the use of a magnetic electrospun chitosan nanofiber composite for hyperthermia treatment of tumor cells. *Acta Biomaterialia, 8*(7), 2704-2711.

Lin, T. C., Lin, F. H., & Lin, J. C. (2013). In vitro characterization of magnetic electrospun IDA-grafted chitosan nanofiber composite for hyperthermic tumor cell treatment. *J Biomater Sci Polym Ed, 24*(9), 1152-1163.

Mahdavi, M., Ahmad, M. B., Haron, M. J., Namvar, F., Nadi, B., Rahman, M. Z., & Amin, J. (2013). Synthesis, surface modification and characterisation of biocompatible magnetic iron oxide nanoparticles for biomedical applications. *Molecules, 18*(7), 7533-7548.

Majewski, P., & Thierry, B. (2007). Functionalized Magnetite Nanoparticles—Synthesis, Properties, and Bio-Applications. *Critical Reviews in Solid State and Materials Sciences, 32*(3-4), 203-215.

Massart, R. (1980). Magnetic fluids and process for obtaining them. USA: Agence National de Valorisation de la Recherche ANVAR

Palma, S. I., Marciello, M., Carvalho, A., Veintemillas-Verdaguer, S., Morales Mdel, P., & Roque, A. C. (2015). Effects of phase transfer ligands on monodisperse iron oxide magnetic nanoparticles. *J Colloid Interface Sci, 437*, 147-155.

Qiu, K., He, C., Feng, W., Wang, W., Zhou, X., Yin, Z., Chen, L., Wang, H., & Mo, X. (2013). Doxorubicin-loaded electrospun poly(l-lactic acid)/mesoporous silica nanoparticles composite nanofibers for potential postsurgical cancer treatment. *Journal of Materials Chemistry B, 1*(36), 4601-4611.

Rao, K. M., Kumar, A., & Han, S. S. (2017). Polysaccharide-based magnetically responsive polyelectrolyte hydrogels for tissue engineering applications. *Journal of Materials Science & Technology*.

Shi, J., Kantoff, P. W., Wooster, R., & Farokhzad, O. C. (2017). Cancer nanomedicine: progress, challenges and opportunities. *Nat Rev Cancer, 17*(1), 20-37.

Soares, P. I., Alves, A. M., Pereira, L. C., Coutinho, J. T., Ferreira, I. M., Novo, C. M., & Borges, J. P. (2014a). Effects of surfactants on the magnetic properties of iron oxide colloids. *J Colloid Interface Sci, 419*, 46-51.

Soares, P. I., Lochte, F., Echeverria, C., Pereira, L. C., Coutinho, J. T., Ferreira, I. M., & Novo, C. M. (2015a). Thermal and magnetic properties of iron oxide colloids: influence of surfactants. *Nanotechnology, 26*(42), 425704.

Soares, P. I., Lochte, F., Echeverria, C., Pereira, L. C., Coutinho, J. T., Ferreira, I. M., Novo, C. M., & Borges, J. P. (2015b). Thermal and magnetic properties of iron oxide colloids: influence of surfactants. *Nanotechnology, 26*(42), 425704.

Soares, P. I., Machado, D., Laia, C., Pereira, L. C., Coutinho, J. T., Ferreira, I. M., Novo, C. M., & Borges, J. P. (2016a). Thermal and magnetic properties of chitosan-iron oxide nanoparticles. *Carbohydr Polym, 149*, 382-390.

Soares, P. I. P., Alves, A. M. R., Pereira, L. C. J., Coutinho, J. T., Ferreira, I. M. M., Novo, C. M. M., & Borges, J. P. M. R. (2014b). Effects of surfactants on the magnetic properties of iron oxide colloids. *Journal of colloid and interface science, 419*, 46-51.

Soares, P. I. P., Laia, C. A. T., Carvalho, A., Pereira, L. C. J., Coutinho, J. T., Ferreira, I. M. M., Novo, C. M. M., & Borges, J. P. (2016b). Iron oxide nanoparticles stabilized with a bilayer of oleic acid for magnetic hyperthermia and MRI applications. *Applied Surface Science, 383*, 240-247.

Talelli, M., Rijcken, C. J., Lammers, T., Seevinck, P. R., Storm, G., van Nostrum, C. F., & Hennink, W. E. (2009). Superparamagnetic iron oxide nanoparticles encapsulated in biodegradable thermosensitive

polymeric micelles: toward a targeted nanomedicine suitable for image-guided drug delivery. *Langmuir, 25*(4), 2060-2067.

Tarus, B., Fadel, N., Al-Oufy, A., & El-Messiry, M. (2016). Effect of polymer concentration on the morphology and mechanical characteristics of electrospun cellulose acetate and poly (vinyl chloride) nanofiber mats. *Alexandria Engineering Journal, 55*(3), 2975-2984.

Thakkar, S., & Misra, M. (2017). Electrospun polymeric nanofibers: New horizons in drug delivery. *European Journal of Pharmaceutical Sciences, 107*, 148-167.

Valois, C. R., Braz, J. M., Nunes, E. S., Vinolo, M. A., Lima, E. C., Curi, R., Kuebler, W. M., & Azevedo, R. B. (2010). The effect of DMSA-functionalized magnetic nanoparticles on transendothelial migration of monocytes in the murine lung via a beta2 integrin-dependent pathway. *Biomaterials, 31*(2), 366-374.

Wu, W., Wu, Z., Yu, T., Jiang, C., & Kim, W. S. (2015). Recent progress on magnetic iron oxide nanoparticles: synthesis, surface functional strategies and biomedical applications. *Sci Technol Adv Mater, 16*(2), 023501.

Yadollahpour, A., & Hosseini, S. A. (2016). Magnetic nanoparticle based hyperthermia: A review of the physiochemical properties and synthesis methods. *International Journal of Pharmaceutical Research and Allied Sciences, 5*(2), 242-246.

Yan, H., Shang, W., Sun, X., Zhao, L., Wang, J., Xiong, Z., Yuan, J., Zhang, R., Huang, Q., Wang, K., Li, B., Tian, J., Kang, F., & Feng, S. S. (2018). "All- in- One" Nanoparticles for Trimodality Imaging- Guided Intracellular Photo- magnetic Hyperthermia Therapy under Intravenous Administration. *Advanced Functional Materials, 28*(9), 1705710.

Yang, K., Peng, H., Wen, Y., & Li, N. (2010). Re-examination of characteristic FTIR spectra of secundary layer in bilayer oleic acid-coated Fe_3O_4 naoparticles. *Applied Surface Science, 256*(10), 3093-3097.

Zhong, Y., Leung, V., Wan, L. Y., Dutz, S., Ko, F. K., & Hafeli, U. O. (2015). Electrospun magnetic nanofibre mats - A new bondable biomaterial using remotely activated magnetic heating. *Journal of Magnetism and Magnetic Materials, 380*, 330-334.
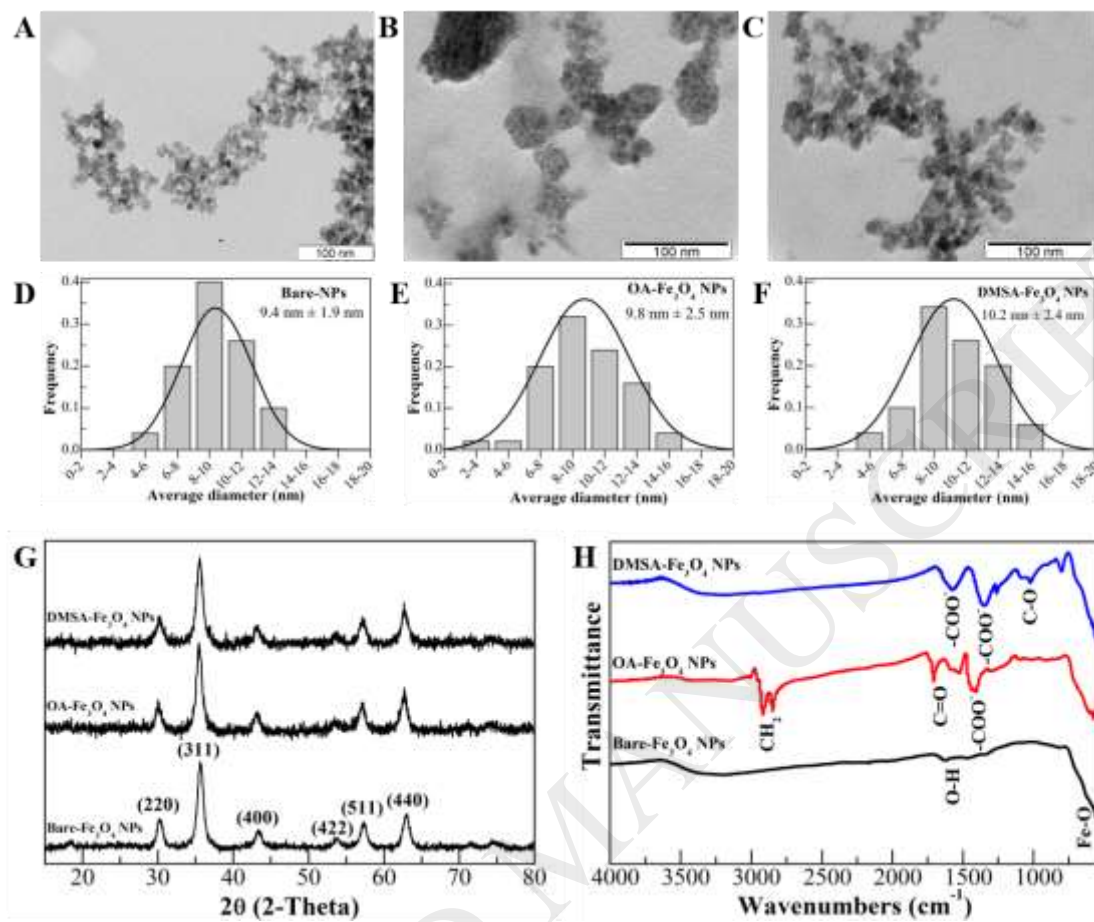
Figures captions

Fig. 1. TEM image and the respective size distribution graph of bare-Fe$_3$O$_4$ NPs (A, D), OA-Fe$_3$O$_4$ NPs (B, E), and DMSA-Fe$_3$O$_4$ NPs (C, F). XRD patterns (G) and FTIR spectra (H) of bare-Fe$_3$O$_4$ NPs, OA-Fe$_3$O$_4$ NPs and DMSA-Fe$_3$O$_4$ NPs.
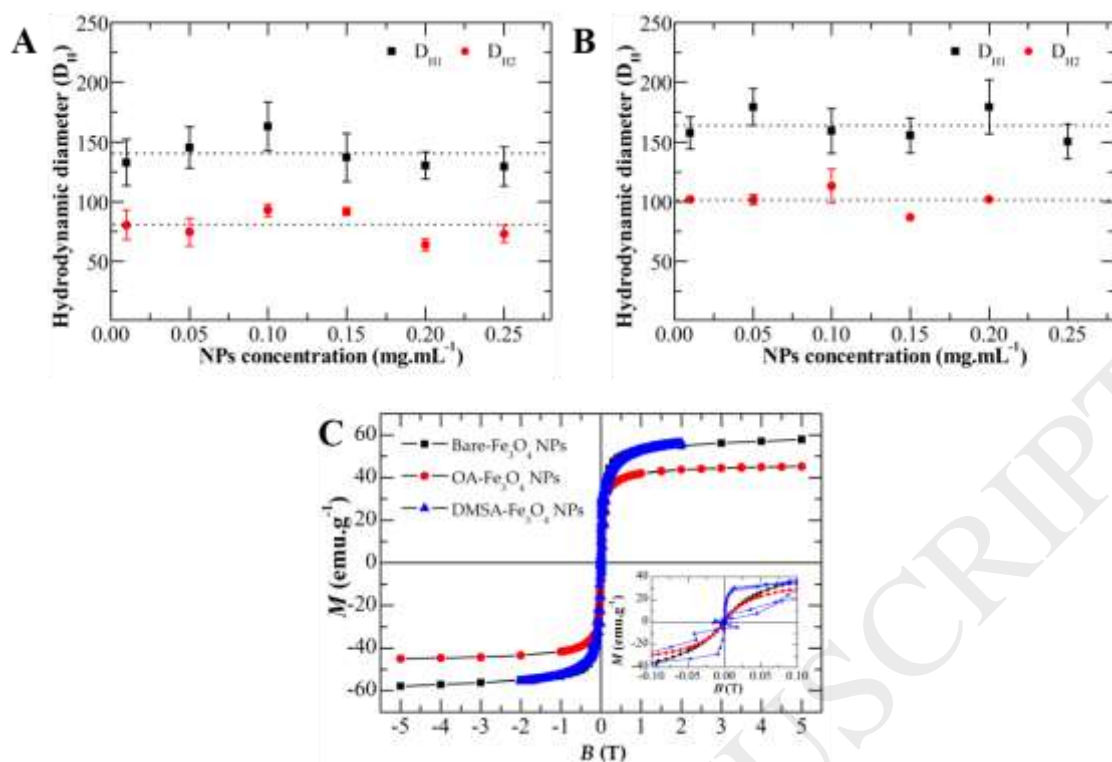
Fig. 2. Hydrodynamic diameter calculated for OA-Fe$_3$O$_4$ NPs (A) and DMSA-Fe$_3$O$_4$ NPs (B). Dashed lines indicate the average diameter for each set of points. The calculated D$_H$ was obtained using the above-described method of the cumulants expansion. Mean ± standard deviation for 5 determinations is shown. Magnetization vs. applied magnetic field (C) for bare-Fe$_3$O$_4$ NPs at 320 K (black), OA-Fe$_3$O$_4$ NPs at 320 K (red), and DMSA-Fe$_3$O$_4$ NPs at 300 K (blue).
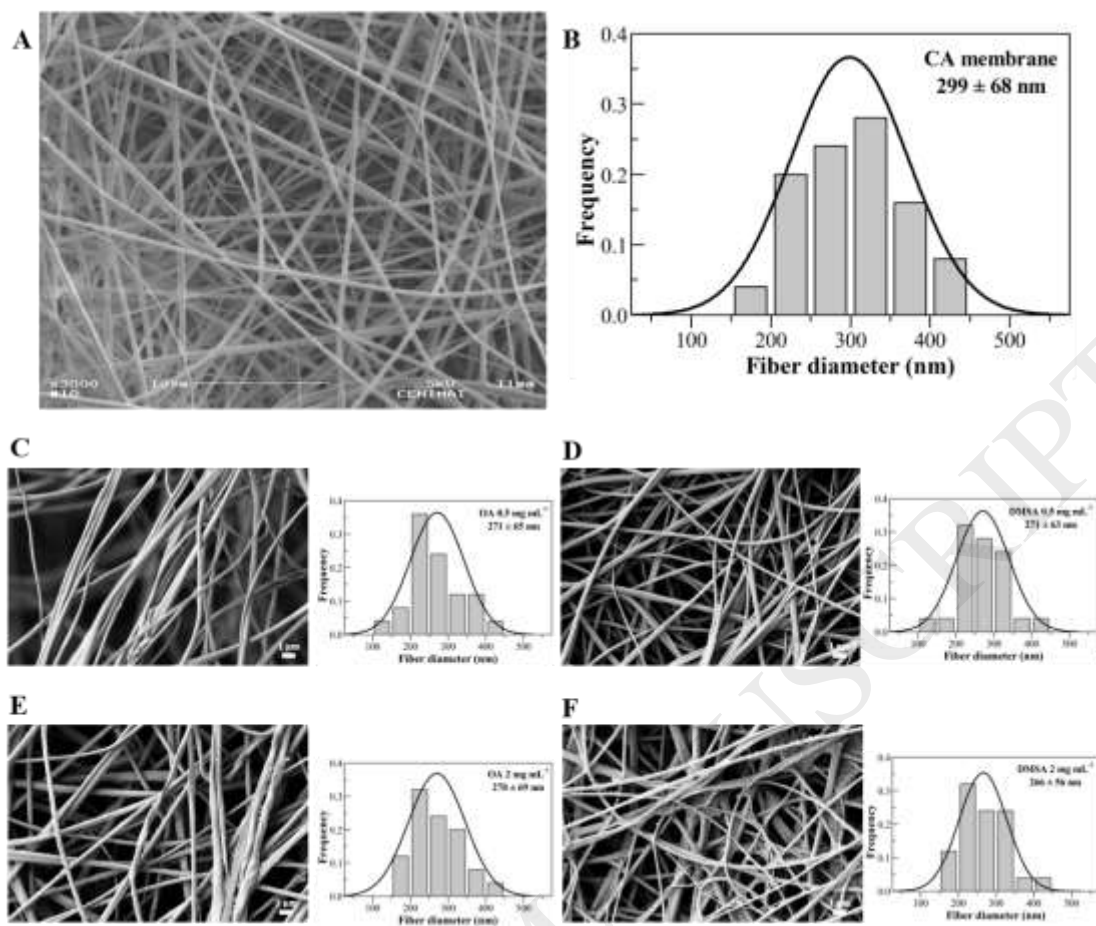
.

Fig. 3. SEM images and the respective fiber diameter distribution graph of CA membrane before Fe_3O_4 NPs adsorption (A, B), and after 24 h of adsorption in OA (C, E) or DMSA (D, F) Fe_3O_4 NPs solution in two concentrations: 0.5 mg.mL^{-1} and 2 mg.mL^{-1}.
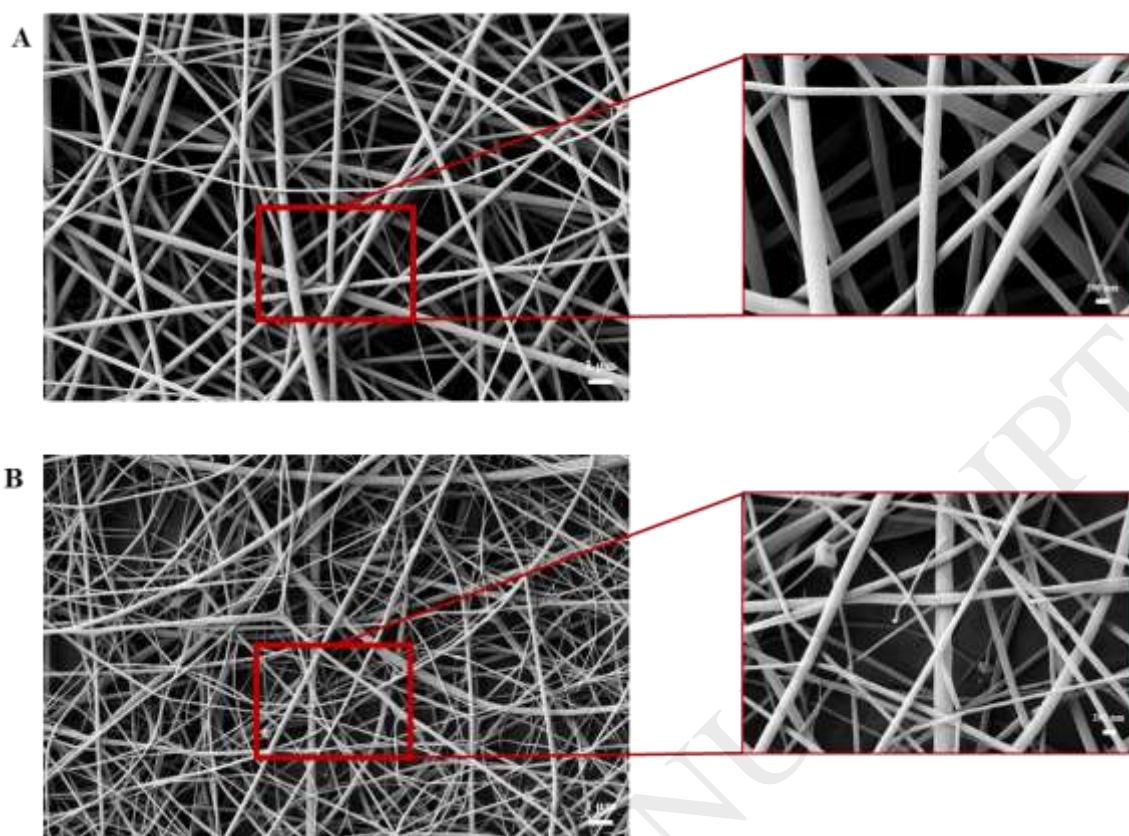
Fig. 4. SEM image of composite CA/Fe$_3$O$_4$ membranes produced by incorporation of OA-Fe$_3$O$_4$ NPs (A) or DMSA-Fe$_3$O$_4$ NPs (B) in the electrospinning solution.
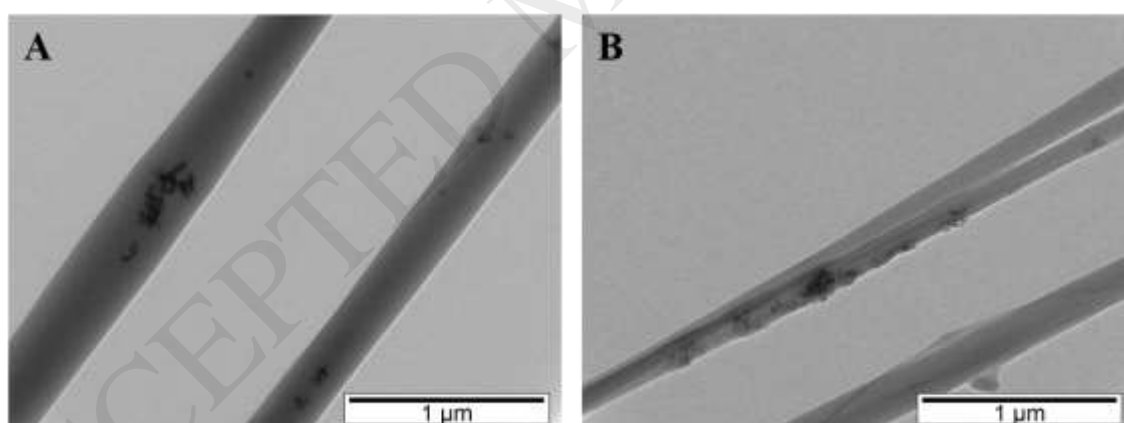
Fig. 5. TEM images of composite CA/Fe$_3$O$_4$ membranes produced by incorporation of OA-Fe$_3$O$_4$ NPs (A) or DMSA-Fe$_3$O$_4$ NPs (B) in the electrospinning solution.
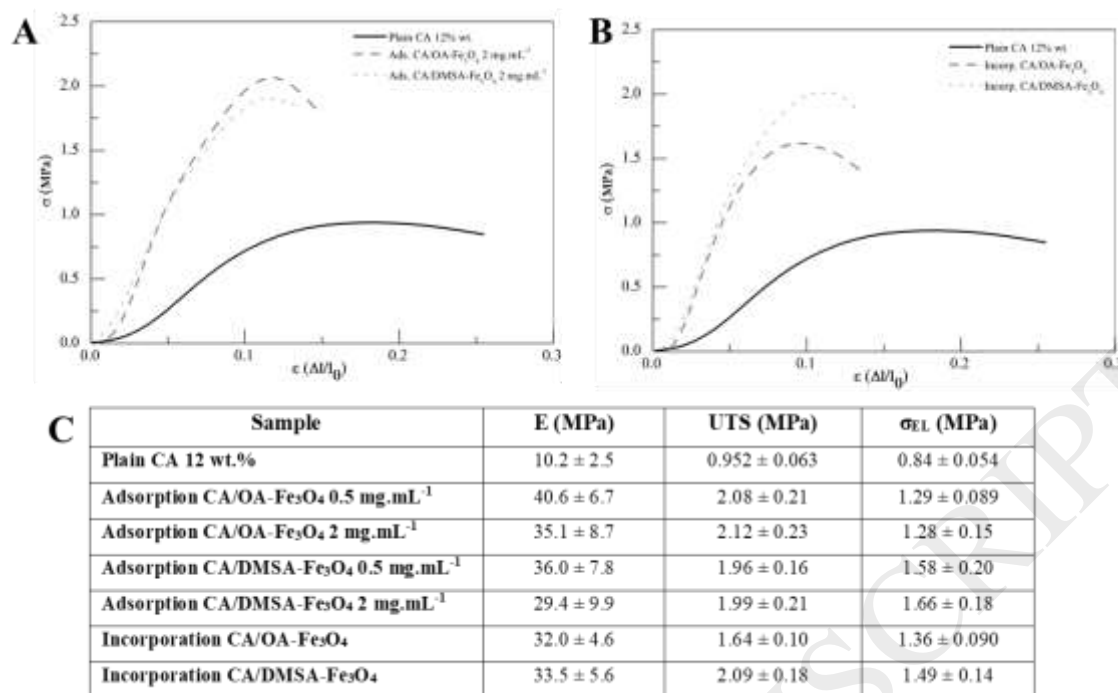
Fig. 6. Representative stress-strain curves of composite membranes produced by physical adsorption at the fibers' surface (A) or by incorporation in the electrospinning solution (B) of OA- and DMSA-Fe_3O_4 NPs, compared to plain CA membrane. (C) Calculated mechanical parameters for each membrane type: Young's modulus (E), ultimate tensile strength (UTS) and elastic limit stress (σ_{LE}).

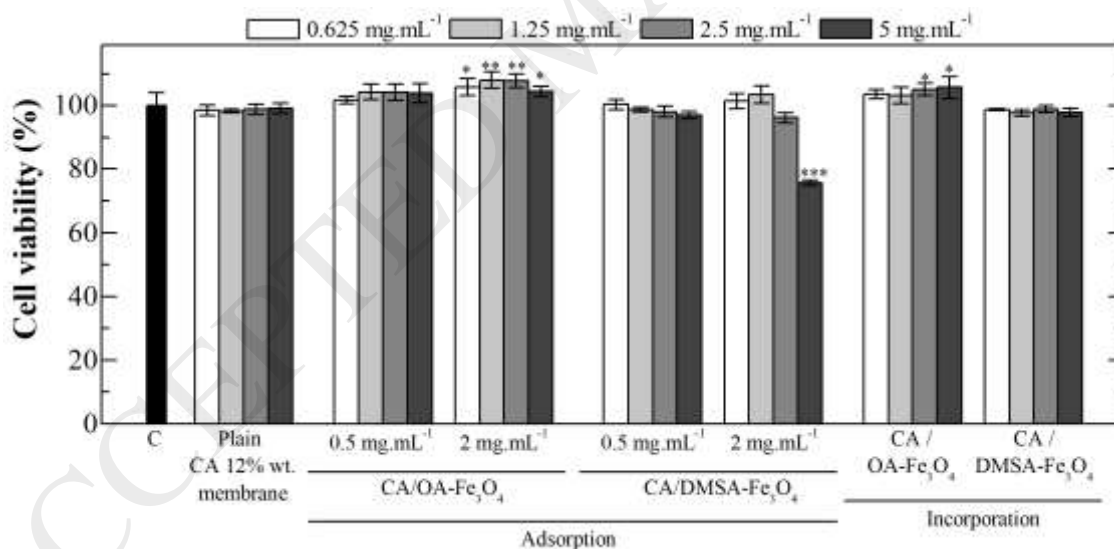| Sample	E (MPa)	UTS (MPa)	σ_{EL} (MPa)
Plain CA 12 wt.%	10.2 ± 2.5	0.952 ± 0.063	0.84 ± 0.054
Adsorption CA/OA-Fe_3O_4 0.5 mg.mL^{-1}	40.6 ± 6.7	2.08 ± 0.21	1.29 ± 0.089
Adsorption CA/OA-Fe_3O_4 2 mg.mL^{-1}	35.1 ± 8.7	2.12 ± 0.23	1.28 ± 0.15
Adsorption CA/DMSA-Fe_3O_4 0.5 mg.mL^{-1}	36.0 ± 7.8	1.96 ± 0.16	1.58 ± 0.20
Adsorption CA/DMSA-Fe_3O_4 2 mg.mL^{-1}	29.4 ± 9.9	1.99 ± 0.21	1.66 ± 0.18
Incorporation CA/OA-Fe_3O_4	32.0 ± 4.6	1.64 ± 0.10	1.36 ± 0.090
Incorporation CA/DMSA-Fe_3O_4	33.5 ± 5.6	2.09 ± 0.18	1.49 ± 0.14

Fig. 7. Vero cell line viability after 24 h exposure to different types of CA membranes through indirect method. Data is expressed as average ± standard deviation for at least five independent experiments. *$p<0.05$, **$p<0.005$, ***$p<0.001$ compared to untreated control cells (C).
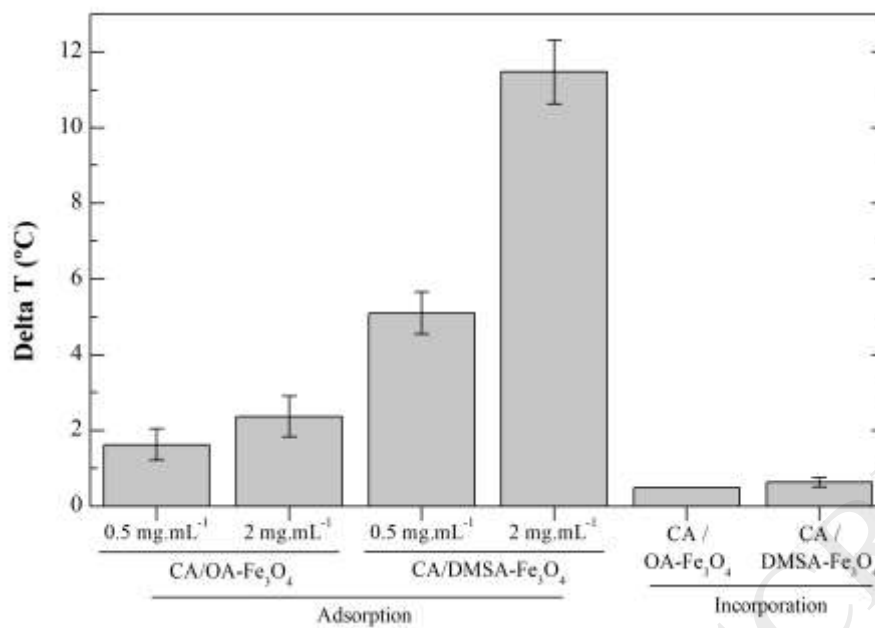
20

Fig. 8. Temperature increase generated by each type of CA membrane with incorporated IONPs during 10 minutes of an AC magnetic field application with magnetic flux density of 300 G and 418.5 kHz of frequency.

Tables

Table 1. Electrospinning parameters tested that resulted in fibers without defects, and the respective average fiber diameter.

Temperature (°C)	Humidity (%)	Flow Rate (ml.h^{-1})	Distance (cm)	Potential (kV)	Average fiber diameter (nm)
22.7	46	0.2	15	20	387 ± 98
20.5	41	0.2	15	20	329 ± 119
22.5	32	0.2	15	20	308 ± 90
21.9	37	0.2	15	20	345 ± 113
20.9	43	0.2	15	20	375 ± 113
20.5	41	0.2	15	17	366 ± 109
20.8	41	0.2	11	20	468 ± 110
21.0	41	0.15	11	20	485 ± 136
21.8	40	0.15	15	20	340 ± 95
21.8	40	0.15	17	20	299 ± 68
21.8	46	0.2	17	20	392 ± 105

Table 2. Parameters used for CA nanomembranes production.

NPs solution	[CA] (wt%)	Temperature (°C)	Humidity (%)	Flow rate (mL.h^{-1})	Distance (cm)	Potential (kV)
-	**12**	**21.8**	**40**	**0.15**	**17**	**20**
OA-Fe_3O_4 NPs	11	25.8	44	0.25	20	20
DMSA-Fe_3O_4 NPs	10	23.7	40	0.20	17	20